doi: 10.56761/EFRE2022.C3-P-037702

The effect of annealing in air on the physicochemical properties of CeF_3 nanoparticles produced by pulsed electron evaporation

V. Ilves[1,], O. Malova[1,2], A. Murzakaev[1,2], T. Sultanova[2], S. Sokovnin[1,2], M. Uimin[2,3], M. Ulitko[2], M. Zuev[2,4]*

[1]*Institute of Electrophysics, UB RAS, Yekaterinburg, Russia*
[2]*Ural Federal University, Yekaterinburg, Russia*
[3]*M.N. Mikheev Institute of Metal Physics, UB RAS, Yekaterinburg, Russia*
[4]*Institute of Solid State Chemistry Ural Branch RAS, Yekaterinburg, Russia*
[*]*ilves@iep.uran.ru*

Abstract. The present work continues to investigate the physicochemical characteristics of CeF_3 nanopowder (NP) produced using the method of pulsed electron beam evaporation (PEBE) in vacuum. The resulting NP was isothermally annealed in air at the temperature of 200, 300 and 500 °C for 30 minutes. XRD showed that the cubic phase CeO_2 formed in NP CeF_3 after annealing at the temperature of 500 °C. The intensity of photoluminescence of NP CeF_3 decreased non-monotonically with an increase in the annealing temperature, the appearance of the oxide phase CeO_2 led to an increase in the intensity of photoluminescence. The paramagnetic response of the NP decreased after annealing. The addition of not annealed NP CeF_3 to tumor culture HeLa and non-neoplastic Vero culture resulted in a 20–35% reduction in cell viability at all NP concentrations in the aqueous suspension. The obtained data show the low cytotoxicity of NP CeF_3 to tumor and non-tumor cells. Improved texture parameters indicate the prospect of using CeF_3 as a nanocontainer to deliver various dosage forms in biomedicine.

Keywords: CeF_3 NPles, annealing in air, pulsed electron beam evaporation.

1. Introduction

Numerous experimental [1] and theoretical works [2] confirm the presence of ferromagnetism at room temperature in cerium oxide NPles (NPles). Prospects for the use of NPles CeO_2 in biomedicine are shown in a number of comprehensive reviews [2] and monographs [3]. No less interesting are the prospects for the use of NPles fluorides, in particular CeF_3, in medicine [4]. Recently, [5] showed that composite NPles CeO_2/CeF_3 (composites were synthesized by fluorination of initial CeO_2 NPles) showed increase of the saturation magnetization in the CeO_2/CeF_3 NPles compared to the initial, vacuum, and air annealed CeO_2 NPles. По мнению авторов [5], the most plausible explanation of the origin of ferromagnetism in composite CeO_2/CeF_3 powder consists in the presence of defects in the interface between composite CeO_2 and CeF_3 structures. Based on the above idea of the origin of RTFM on the "fluoride oxide" interface of the composite, we decided to test the possibility of an FM response as a result of the formation of an oxide shell from CeO_2 during annealing in air on the surface of paramagnetic NPles CeF_3 after their annealing in air (previously, we experimentally observed FM response in NPles pure CeO_2 and Cu (C, Fe) doped CeO_2 [6] and paramagnetism NPles CeFe [7]). Early studies of phase transformation of CeF_3 during annealing in air [8] showed that a noticeable amount of CeO_2 is formed in the CeF_3 powder only after annealing at the temperature of 600–700 °C, which was confirmed by X-ray diffraction (XRD) analysis. We decided to anneal in air the NPles CeF_3 produced earlier by the PEBE method in vacuum [7], in order to induce in NPles CeF_3-CeO_2 FM on the "fluoride-oxide" interface without using gas fluorination, and in parallel to study the physicochemical characteristics of the annealing core-shell NPles CeF_3 (core) -CeO_2 (shell). Studies of nucleus-shell structures show their intense luminescence and biocompatibility [9]. The core-shell structures are attractive due to their remarkable physicochemical characteristics, such as thermal stability, improved solubility in water, etc. [10]. In turn, the luminescent and magnetic properties of NPles lanthanides play a fundamental important role in the design of multifunctional nanomaterials, allowing them to be used in magnetic resonance therapy and other luminescent methods, including for deep tissue

imaging and low-resolution imaging [11]. The results of the present work showed that air annealing of NPles CeF_3 did not lead to an FM response on the «fluoride-oxide» interface.

2. Experimental

Cerium(III) fluoride micron powder (CeF_3, anhydrous, powder, 99.99% trace metals basis, Sigma-Aldrich, #229555) was used for producing CeF3 NPles. Mesoporous amorphous crystal NP CeF_3 was prepared by PEBE method [7]. Annealing of micron and nano powders CeF_3 was carried out in air at 200, 300 and 500 °C. The evolution of the color of NP CeF_3 from the annealing temperature is shown in Fig.1a. NP, after annealing at 500 °C, acquired a brighter color than the color of unannealed micron powder (sample SM0). The change in NP color indirectly proves that the dark color (the color of NP-coffee with milk) of the original NP CeF_3 (sample S0) was not caused by an impurity of an unspecified oxofluoride phase, but was associated with a large number of all kinds of structural defects and a small amount of metal NPles Ce recovered by evaporation at high temperature under vacuum conditions. A similar evolution of the NP color was observed by us earlier during annealing in the air of NP CaF_2, also obtained by PEBE in vacuum [12]. A change in the color of micron powder with an increase in the annealing temperature (Fig.1b) was not visually observed. The X-ray diffractogram was taken on the D8 DISCOVER diffractometer. Nitrogen adsorption and desorption isotherms at 77 K were obtained using Micromeritics TriStar 3000 V6.03 A. Thermal analysis of the sample NP CeF3 was carried out on complex NETZSCH STA-409. Magnetic measurements were carried out using a Faraday balance. The cytotoxicity of CeF_3 NPs (from stainless steel) and CeF3 (glass substrates) was tested in human and animal cell cultures: Vero green monkey cell culture and HeLa human tumor culture.

Fig.1 The evolution of the color of NP CeF_3 from the annealing temperature: a – change of the color of the NP CeF_3 (sample S0) from the annealing temperature in air; b – color change of SM sample from commercial powder (Cerium (III) fluoride, anhydrous powder, 99.99% trace metal basis, Sigma-Aldrich) from air annealing temperature.

3. Results and discussion

X-ray diffractograms of the original unannealed micro and nano powders CeF_3 (samples SM and S0) and annealed at 200, 300 and 500 °C NP S0 (samples S200,S300 and S500) are shown in Fig.2. Commercial powder (Fig.1a) contained one hexagonal phase CeF_3, S.G.: P63/mcm (193), OSR = 87 (3) nm, periods a = 7.129 (4) Å, c = 7.285 (5) Å, ρ = 6.125 (4) g/cm^3. (PDF No. 01-089-1933). The unannealed CeF_3 NP contained two phases: – hexagonal phase CeF_3, S.G.: P63/mcm (193); content ≈ 95 wt%, CSR ≈ 8 nm, periods a = 7.12(2) Å, c = 7,29(2) Å, ρ = 6.15(4) g/cm^3, (PDF No. 01-089-1933) and impurity cubic phase [Ce-O-F] or [Ce-F], content ≈ 5% (weight), CSR = 31 (3) nm, period a = 5.76 (2) Å, ρ = 6.07 (5) g/cm^3. Crystal lattice parameters and CSR size

of samples S200 and S300 are given in Table 1. Annealing of sample S0 at 500 °C (Table 2) resulted in the formation of NPles cerium oxide (Cerianite , S.G.: Fm-3m (225), map PDF No. 00-034-0394), comparable in size CSR with hexagonal NPles CeF_3 (CeF_3, S.G.: P63/mcm (193) map PDF No. 01-089-1933).

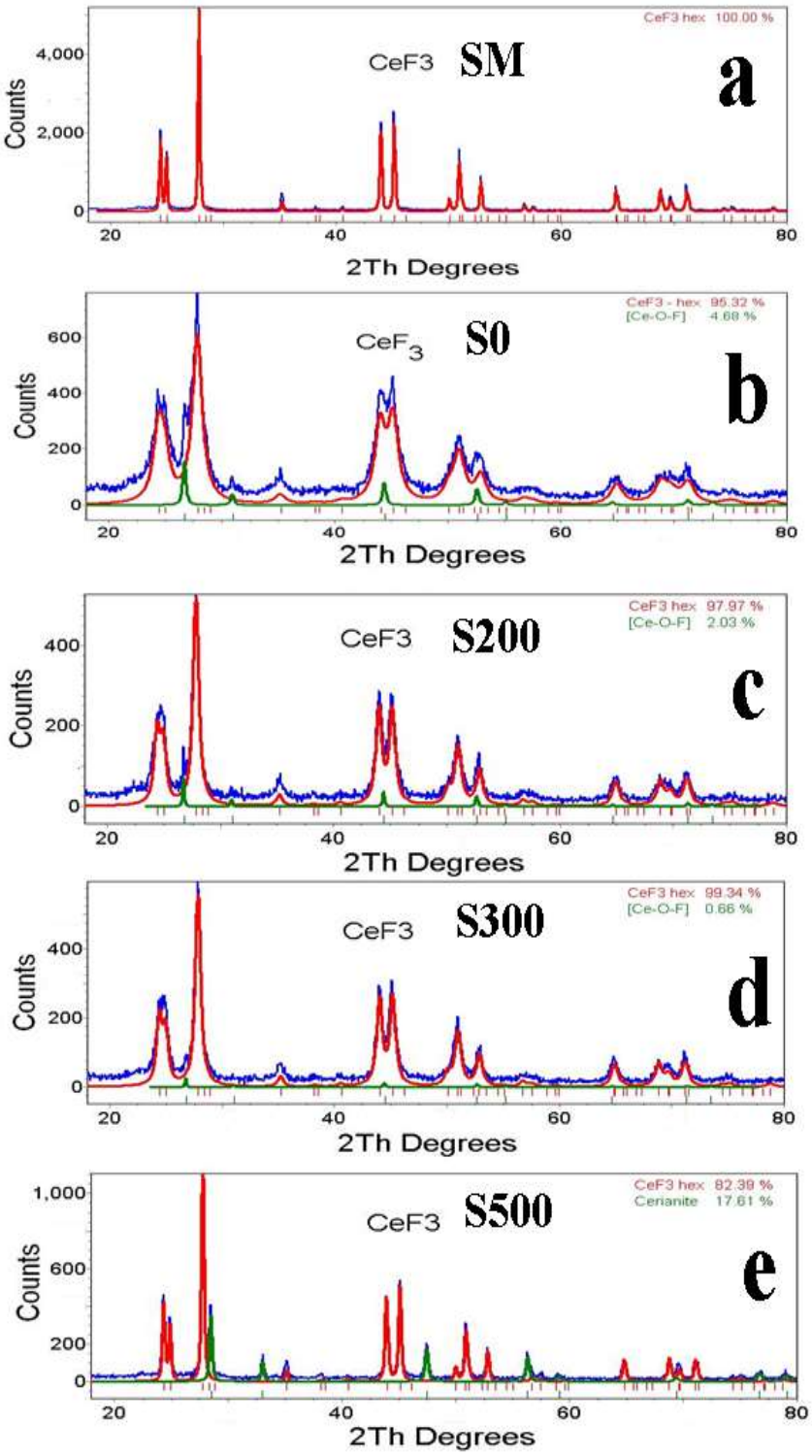

Fig. 2 XRD pattern of unannealed (micro and nano powders) (a, b) and in air annealed at 200, 300 and 500 °C CeF_3 powders (c–e).

Table 1. Crystal lattice parameters and CSR dimensions of the hexagonal phase CeF_3 in annealed samples of S200 and S300

Sample	$CeF_{3\ hex}$			
	Concentration, %*	CSR, nm	Period, Å	ρ, g/cm³
S200	≈ 98	15(2)	a = 7.121(3) c = 7.278(3)	6.144(2)
S300	> 99	16(2)	a = 7.124(3) c = 7.282(3)	6.136(2)

* phase [Ce-O-F] or [Ce-F], about 1–2 wt.% (PDF card No. 01-075-0249, S.G.: Fm-3m, cubic, period a = 5.703 Å, ρ = 6.271 g/cm³)

Table 2. Crystal lattice parameters and CSR dimensions of the hexagonal phase of the CeF_3 and cubic phase CeO_2 in the sample S500

CeF_3				CeO_2			
Concentr., %	CSR, nm	Period, Å	ρ , g/cm³	Concentr.%	CSR, nm	Period, Å	ρ, g/cm³
≈ 82	50(2)	a = 7.129(3) c = 7.285(3)	6.124(3)	≈ 18	44(2)	a = 5.411(2)	7.215(3)

In [13], NPles CeF_3 with an average nanocrystal size of 9.6 nm comparable to the NPles (CSR ≈ 8 nm) in sample S0, were annealed in air at 350 °C for 1 hours and at 500 °C for 6 hours. The particle sizes after annealing were 17.6 and 63.7 nm. The NPles CeF_3 sizes in our samples of S300 and S500 annealed in air for 0.5 hours were 16 and 50 nm, respectively, indicating approximately the same growth rate of the CeF_3 nanocrystals at a comparable size of the starting particles. In [13] also recorded the formation of CeO_2 oxide (concentration 30%, particle size 75 nm) during annealing of the sample at the temperature of 500 °C, which is well consistent with our XRD data. The morphological analysis of NPles CeF_3 produced in vacuum by PEBE was carried out by us earlier (see Fig.3 in SUPP.MATER in [6]) using low-resolution (TEM) and high-resolution transmission electron microscopy (HRTEM). Briefly, the produced NPles were mesoporous agglomerates of particles (agglomerate size several hundred nm) consisting of amorphous-crystalline particles, from ultrasmall size (2–3 nm) to large particles, 15–16 nm in size, with an irregular, ellipsoid shape, without a clear cut. The selected area electron diffraction (SAED) patterns are consistent with a hexagonal phase structure of CeF_3 with strong ring patterns due to (002), (110), (111), (300), (113), (200), (302) and (221) planes, in good agreement with XRD patterns. Fig.4 shows isotherms of adsorption-desorption of trifluoride (micro and nano sizes) and their pore size distribution.

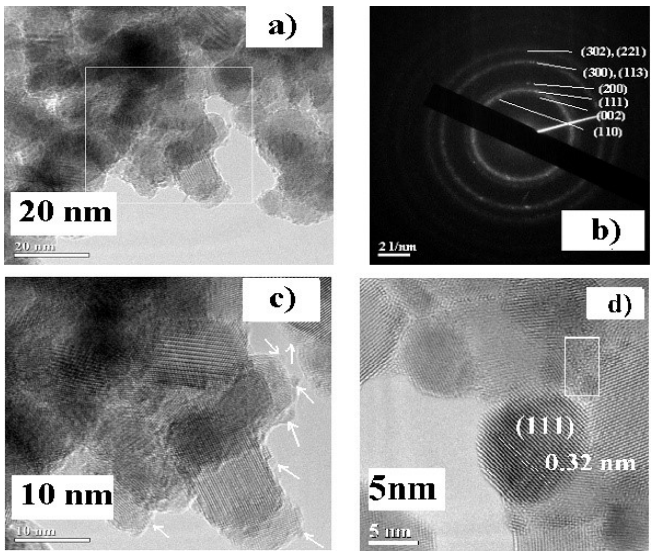

Fig.3. Morphological analysis of NPles CeF_3: a – TEM; c, d – HRTEM images and b – SAED pattern of CeF_3 NPles. The area highlighted by a white rectangle in Fig.3a is shown in Fig.3c. The amorphous area of the sample in Fig.3d is marked with a white rectangle [7].

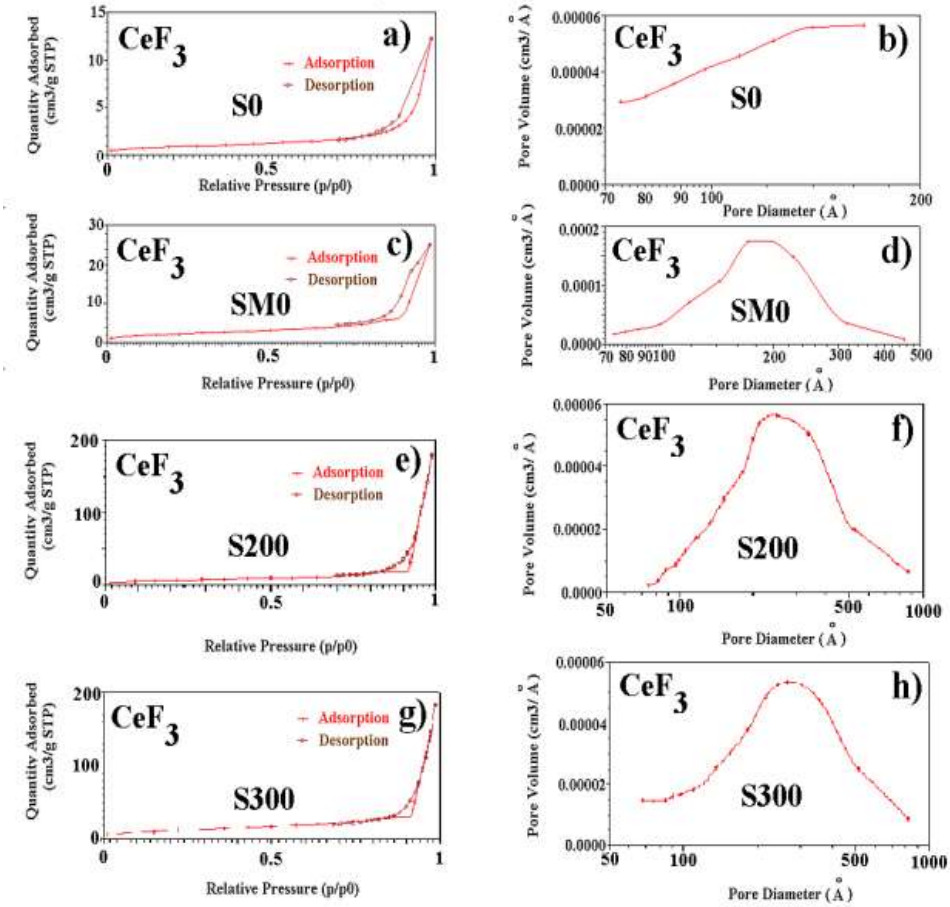

Fig. 4. Nitrogen adsorption/desorption isotherms (a, e, g) and pore size distribution curves (b, f, h) of samples S0, S200, S300 and commercial micron powder Ce F_3 (c) and (d) , respectively.

The nitrogen isotherms of samples S0 and SM0 in (Fig.4a and 4c) belong to the IV type with an H3 hysteresis. The specific surface area (SSA) and texture parameters of the initial and annealed powders are given in Table 3. The SSA of the non-annealed NP CeF3 (sample S0) is nearly 8 times more than the SSA of the commercial sample SM0, with a smaller pore size, the sample has a significantly larger pore volume. Improved textural parameters of CeF_3 nanopowder indicate its possible use as a nanocontainer for drug delivery, as confirmed by recent studies [4].

Table 3. Texture parameters of non-annealed and air-annealed samples of micro and nano powders CeF_3

Samples	SSA, m^2/g	Pore Size, nm	Pore Volume, cm^3/g
SM0	7.2	21.5	0.04
S0	62.0	12.3	0.11
S200	25.1	33.7	0.28
S300	44.5	32.3	0.28
S500	–	–	–

Ha Fig.5a and 5b shows the DSC-TG synchronous heating curve and H_2O, CO_2 mass spectra of the sample CeF_3 NP and commercial powder in the temperature range 40–1400 °C in argon atmosphere, respectively. Three thermal peaks are clearly visible on the DSC heating curve of NP CeF_3 (Fig.5a): endothermic peak *1* in the range of 40–250 °C was caused by evaporation of adsorbed water. The thermal stability of the CeF_3 sample after heating to the temperature 730 °C was possibly disturbed, as indicated simultaneously by an exothermic peak *2* on the DSC curve (730–1170 °C). Most probable that the exothermic peak *2* could be caused by evaporation from the

surface and from the pores of the sample impurity – cerium tricarbonate (melting temperature of $Ce_2(CO_3)_3$ is 610 °C). A large exothermic peak *3* in the temperature range from 1170 to 1400 °C (Fig.5a) is associated with the phase transformation of the metastable hexagonal phase CeF_3 into a more stable at high temperature x-CeF_3 phase.

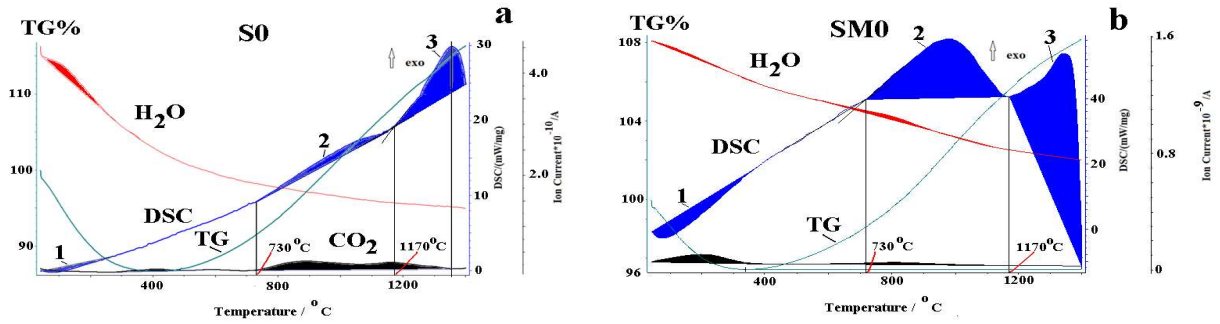

Fig.5. Thermal peaks: a – synchronous heating curves DSC-TG and H_2O, CO_2 mass spectra of CeF_3 NP in the temperature range 40–1400 °C in argon atmosphere; b – synchronous heating curves DSC-TG and H_2O, CO_2 mass spectra of commercial powder CeF_3 in the temperature range 40–1400 °C in argon atmosphere.

Three corresponding thermal peaks were present on the commercial powder heating thermogram (Fig.5b). Fig.6 shows the magnetization curves of annealed in air at the temperature 200, 300 and 500 °C NP and commercial power CeF_3.

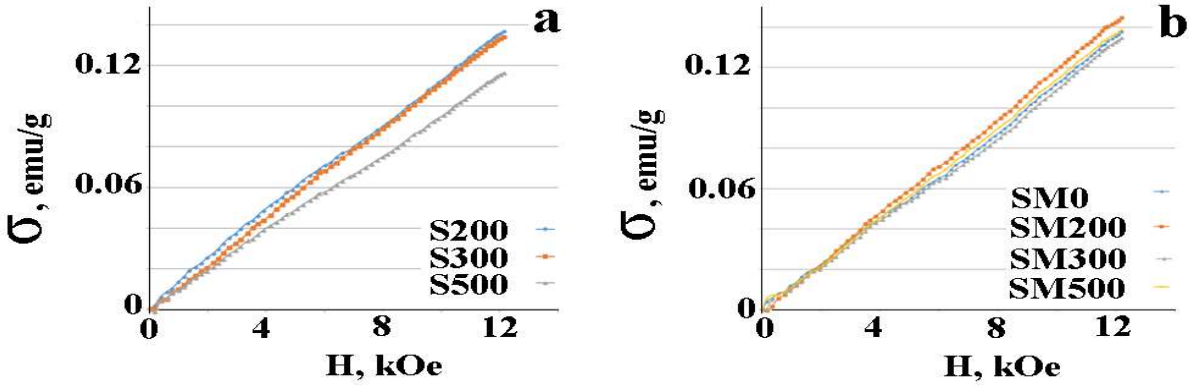

Fig.6. Magnetization curves: a – specific magnetization of CeF3 NPles annealed in air at temperatures of 200, 300 and 500 °C; b – specific magnetization of commercial CeF3 powder annealed in air at temperatures of 200, 300 and 500 °C.

Curves of magnetization of CeF_3 NP and commercial powder CeF_3 are linear functions of the field, and the susceptibility size determined by an inclination of curves corresponds to tabular value at the room temperature of $1.1 \cdot 10^{-6}$ cm^3/g, i.e. transition to a nanostate didn't affect magnetic behavior of CeF_3 in any way. Unlike recent work of [5] in which a significant increase in room temperature ferromagnetism was observed in composite NPles of CeO_2/CeF_3, we didn't observe emergence of a ferromagnetic response at the room temperature that can be connected with lack of necessary amount of structural defects on borders of grains – "fluoride-oxide", when forming oxidic particles of CeO_2 on CeF_3 NPles surface when annealing.Photoluminescence spectra (PL) and deconvolution by the Gaussians of unannealed and annealed samples of CeF_3 nanopowder and commercial CeF_3 powder at 200, 300 and 500 °C are shown in the Fig.7.

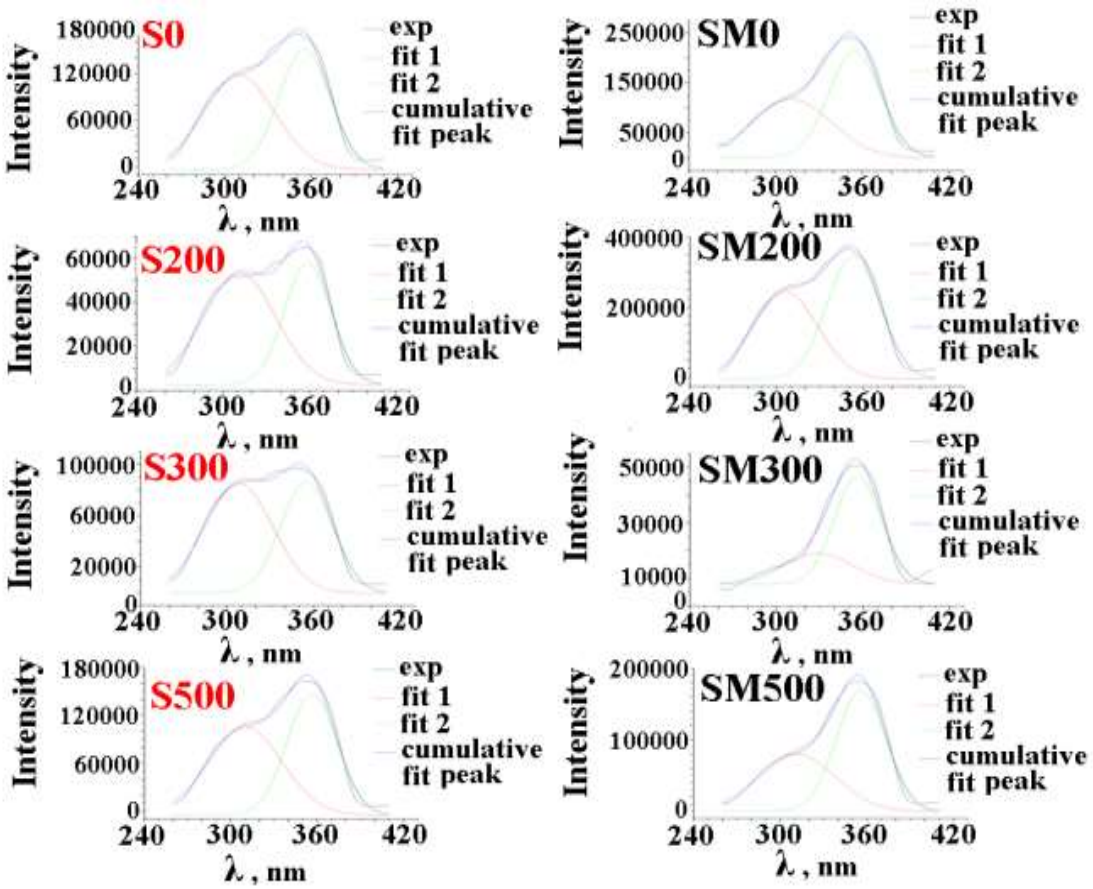

Fig.7 PL spectra of NP and commercial CeF3 powder before and after annealing in air at 200, 300 and 500°C.

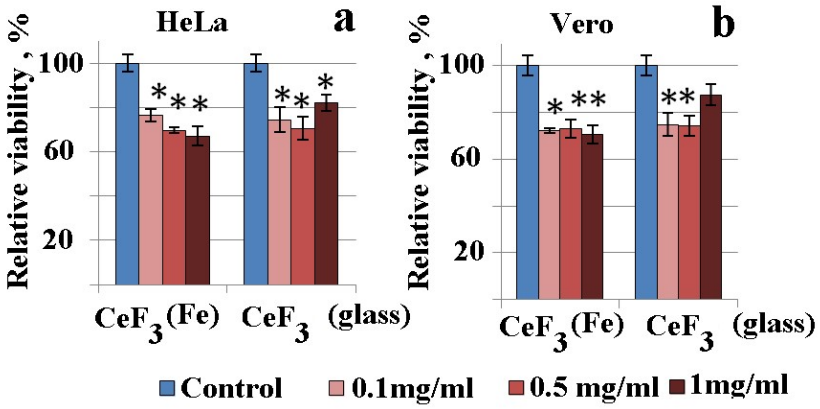

Fig. 8. Change in cell viability when adding CeF3 and CeF3 nanopowders (from glass): a – HeLa cell culture; b – Vero cell culture (* – difference with control is significant ($p < 0.05$)).

The micro and nanopowder spectra contained one wide peak in the range 260 to 390 nm, consisting of two peaks with maxima at ~(308–312) nm (excluding sample SM300) and ~(353–358) nm. Literature data relate both peaks to Ce^{3+} ion emission (transition 5d-4f). According to the results of the experiment, it was found that when CeF_3 nanopowders (from glass) were added to the HeLa tumor culture, the cell viability decreased by 20–35% at all test concentrations (Fig.8). A cytotoxicity study of CeF_3 nanopowder collected from glass and metal substrates showed low cytotoxicity of fluoride NPles in both tumor and non-tumor cells.

4. Conclusion

Annealing of NP CeF_3 in the air led to the formation of two phase NP CeF_3-CeO_2 at the temperature of 500 °C. The volume and pore size of NP after annealing at the temperature of 200–300 °C increased almost 3 times, which makes such powders promising for drug delivery. All NPs CeF3 showed low cytotoxicity in relation to tumor and healthy cells.

Acknowledgments

The work was carried out with the financial support of the Russian Science Foundation, project No. 22-19-00239.

References

[1] Ackland K., Coey J.M.D., *Phys. Rep*., **746**, 1, 2018; doi: 10.1016/j.physrep.2018.04.002
[2] Saifi M.A., Seal S., Godugu C., *J. Control Release*, **338**, 10, 164, 2021; doi: 10.1016/j.jconrel.2021.08.033
[3] Ivanov V.K., Shcherbakov A.B., Baranchikov A.E., Kozik V.V., *Nanocrystalline cerium dioxide: properties, preparation, application.* (Tomsk: Tomsk University Press, 2013).
[4] Shcherbakov A.B., et al., *Mater. Sci. Eng. C*, **50**, 151, 2015; doi: 10.1016/j.msec.2015.01.094
[5] Morozov O.A., et al., *Phys. Stat. Sol. (RRL)*, **12**, 1800318, 2018; doi: 10.1002/pssr.201800318
[6] Ilves V.G., Sokovnin S.Yu, *Nanotech. Russ.*, **7**, 213, 2012; doi: 10.1134/S1995078012030068
[7] Ilves V.G., Sokovnin S. Yu., Uimin M.A., *J. Fluor. Chem.*, **253**, 109921, 2022; doi: 10.1016/j.jfluchem.2021.109921
[8] Lu J., Xue Q., Ouyang J., *Wear, 211*, 1997; https://www.halide-crylink.com/wp-content/uploads/2020/06/12-Thermal-properties-and-tribological-characteristics-of-CeF-3-compact.pdf
[9] Wang J., et al., *ACS Omega*, **5**(30) 19174, 2020; doi:10.1021/acsomega.0c02551
[10] Chaput F., et al., *Langmuir*, **35**, 16256, 2019; doi: 10.1021/acs.langmuir.9b02335
[11] Dong H., et al., *Chem. Rev.*, **115**, 10725, 2015; doi: 10.1021/acs.chemrev.5b00091
[12] Ilves V.G., et al., *Phys. Sol. State.*, **61**, 2200, 2019; doi: 10.1134/S1063783419110179
[13] Mishra S., et al., *Dalton Trans.*, **42**, 12633, 2013; doi: 10.1039/c3dt50605c